Group-Level and Functional-Region Analysis of Electric-Field Shape During Cerebellar Transcranial Direct Current Stimulation with Different Electrode Montages

Jose Gomez-Tames[1], Akihiro Asai[1], Marko Mikkonen[2], Ilkka Laakso[2,3], Satoshi Tanaka[4], Shintaro Uehara[5], Yohei Otaka[6], Akimasa Hirata[1]

1. Department of Electrical and Mechanical Engineering, Nagoya Institute of Technology, Nagoya, Aichi 466-8555, Japan.
2. Department of Electrical Engineering and Automation, Aalto University, Espoo FI-00076, Finland.
3. Advanced Magnetic Imaging Centre, Department of Neuroscience and Biomedical Engineering, Aalto University
4. Hamamatsu University School of Medicine, Hamamatsu, 431-3192, Japan.
5. Faculty of Rehabilitation, Fujita Health University School of Health Sciences, 470-1192, Japan.
6. Department of Rehabilitation Medicine I, Fujita Health University School of Medicine, 470-1192, Japan.

*Corresponding Authors:
Jose Gomez-Tames* and Akimasa Hirata**
Tel & Fax: +81-52-735-7916
*E-mail:jgomez@nitech.ac.jp
** E-mail:ahirata@nitech.ac.jp

Abstract

Objective. Cerebellar transcranial direct current stimulation (ctDCS) is a neuromodulation scheme that delivers a small current to the cerebellum. In this work, we computationally investigate the distributions and strength of the stimulation dosage during ctDCS with the aim of determining the targeted cerebellar regions of a group of subjects with different electrode montages.

Approach. We used a new inter-individual registration method that permitted the projection of computed electric fields (EFs) from individual realistic head models (n = 18) to standard cerebellar template for the first time.

Main Results. Variations of the EF on the cerebellar surface were found to have standard deviations of up to 55% of the mean. The dominant factor that accounted for 62% of the variability of the maximum EFs was the skin–cerebellum distance, whereas the cerebrospinal fluid volume explained 53% of the average EF distribution. Despite the inter-individual variations, a systematic tendency of the EF hotspot emerges beneath the active electrode in group-level analysis. The hotspot can be adjusted by the electrode position so that the most effective stimulation is delivered to a group of subjects.

Significance. Targeting specific cerebellar structures with ctDCS is not straightforward, as neuromodulation depends not only on the placement/design of the electrodes configuration but also on inter-individual variability due to anatomical differences. The proposed method permitted generalizing the EFs to a cerebellum atlas. The atlas is useful for studying the mechanisms of ctDCS, planning ctDCS and explaining findings of experimental studies.

Keywords: Cerebellar Transcranial Direct Current Stimulation; Cerebellum; Inter-individual Variability; Functional Network; Computational Model; Electric Field

1. Introduction

Cerebellar transcranial direct current stimulation (ctDCS) is a form of brain stimulation that modulates human cerebellar activity and behavior [1,2]. The modulation is achieved by the delivery of an electric current (1–2 mA) to the brain via two electrodes placed on the scalp.

Targeting specific brain structures is not straightforward and the mechanisms are yet fully understood for transcranial direct current stimulation. To quantify the electric field (EF), which is a primary determinant of the stimulation/neuromodulation effects (e.g., shift in the membrane potential, synaptic strength mediated in a polarity-dependent manner [3,4]), a computational model is often used. The EF distribution is related not only to the placement and design of the electrodes [5–10], but also to the individual's anatomical features between and beneath the electrodes [11,12]. Consequently, the EF can vary substantially among individuals and its impact on the spatial specificity and efficacy of neuromodulation is unclear [13]. In our previous study [14], we confirmed the effect of dose on motor excitability. Therefore, dosimetry analysis becomes important in the design of the experiment.

As the cerebellum is critical for both motor and cognitive control, ctDCS may be a useful therapeutic intervention for patients with neurological conditions [15–19]. Furthermore, given that each of the cerebellar anatomical subregions likely contributes to a different function, such as the contribution of lobule VI to limb movement or that of the vermis to whole-body posture and locomotion [20–22], activation of different targets can be customized to improve different conditions. To enhance ctDCS intervention, we must know how ctDCS targets cerebellar structures by using different electrode montages.

Computational modeling has been used to investigate the internal EF in anatomical head models for ctDCS [23,24]. Previous studies have shown that EFs are maximal in the targeted cerebellar hemisphere, with little effect on other neural structures [24–26] in a limited number

of subjects. However, our previous study on tDCS [11] suggested a large inter-individual variability of the EF, urging for a systematic analysis of ctDCS by considering group-level effect of the dosage. For that, inter-individual registration and functional network analysis [27,28] of the cerebellum need to be considered for ctDCS planning.

The primary goal of the present study is to investigate the distributions and strength of the internal EF with the aim of determining the targeted cerebellar regions at a group level considering different electrode montages. This approach permitted generalizing the EFs to an average cerebellum (parcellated in seven functional networks) using inter-individual registration methods for the first time. We focused on seven cerebellar functional networks [27,28] and two anatomical regions as the possible subregions targeted by ctDCS. The two anatomical subregions, lobule VI and the vermis, were preliminarily selected because they are potential ctDCS targets for improving primitive motor functions [20–22] in patients with neurological disorders and/or facilitating the planning and efficacy of clinical rehabilitation.

2. Materials and methods

2.1. Head Models

The procedure employed to develop head models from magnetic resonance images (MRIs) has been described in our previous paper [11]. In brief, the FreeSurfer image analysis software [29,30] was used to reconstruct the surfaces of the grey and white matter. Non-brain tissues were segmented from T1- and T2-weighted MRIs with a semi-automatic procedure using the region-growing and thresholding techniques, as described previously [11]. The MRIs had a limited field of view in the neck and, therefore, the images were extended by adding a neck developed by averaging over seven subjects. Please refer to appendix A for more details.

The head models of eighteen subjects were constructed from MRIs (available at

http://hdl.handle.net/1926/1687) and represented by a grid of cubical voxels (4×10^6 voxels with a resolution of 0.5 mm). The mean age of the sample population was 43.4 ± 9.8 yr (all males). The models were segmented into 15 tissues/body fluids: skin, fat, muscle, bone (cancellous/cortical), blood, grey matter, white matter, cerebellar grey matter, cerebellar white matter, brainstem, nuclei, ventricles, cerebrospinal fluid (CSF), and eyes. The CSF was the volume inside the skull that was not explicitly classified as nervous tissue or blood (Fig. 1 (A)).

2.2. Computational Simulation

The scalar-potential finite-difference method [31] was used to solve the scalar-potential equation

$$\nabla\left(\sigma\left(\nabla(\varphi)\right)\right) = 0 \tag{1}$$

where φ and σ denote the scalar potential and tissue conductivity, respectively. The electric conductivity of head tissues was assumed to be linear and isotropic, as shown in Table 1 [32]. The conductivity of skin (innermost part of stratum corneum) is obtained from [33]. We also considered muscle anisotropy, discussed in subsection 3.5, assuming muscle conductivity to be a tensor with off-diagonal elements equal to zero and the longitudinal direction of muscle fibers to be parallel to the superior–inferior direction, as follows.

$$\begin{bmatrix} \sigma_{transversal} & 0 & 0 \\ 0 & \sigma_{transversal} & 0 \\ 0 & 0 & \sigma_{longitudinal} \end{bmatrix} \tag{2}$$

The conductivity ratio (longitudinal/transversal) was 3.5 ± 2 [34–37].

By defining scalar potentials (unknowns) at each node of a cubic voxel (minimum component of the model; 9.1×10^6 voxels in this study), we derived a branch current flowing from one node to a neighboring node along the side of the voxels, which included a scalar potential due to the applied electric charge and impedance between the nodes. By applying Kirchhoff's current law

at all the nodes, we then formed a set of simultaneous equations. We solved the potential iteratively using the multigrid method with successive over-relaxation smoothing [38]. The number of multigrid levels was six, and the iteration continued until the relative residual was smaller than 10^{-6} [38]. To mitigate numerical artifacts resulting from computing the EF with the voxel model at the surface of the CSF–brain boundaries, we suppressed the 99.9th percentile value of the EF [39]. The EF along the edge of the voxel was obtained by dividing the voltage between the nodes of the voxel by the distance across the nodes.

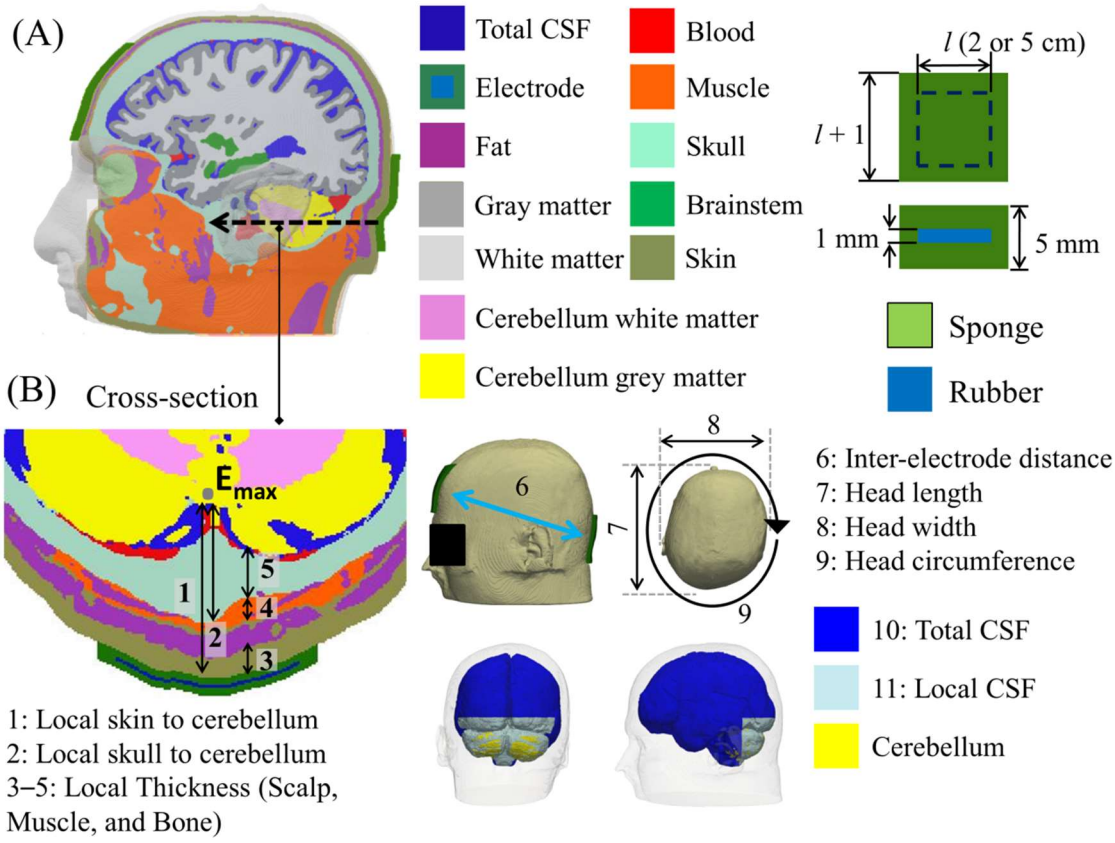

Figure 1. Anatomical head model. (A) Lateral view of the head model, including the cerebellum. (B) Definition of 12 anatomical factors characterizing the EF (the total intracranial volume is not shown here). "Local thickness" refers to the average values over the cerebellar area (similar to local CSF).

The electrodes were square sponges were soaked in normal saline solution (6 × 6 cm^2, 5 mm of thickness, conductivity of 1.6 S/m) [40,41]. A 1-mm-thick rubber sheet (0.1 S/m [40,42]) was inserted in the sponge as shown in Fig. 1 (A). The current source or sink was placed on the top of the rubber. The injected current was 2 mA. The "active electrode" was placed in different positions in the occipital region: one position was centered on the median line over the cerebellum, 2 cm below the inion, while the others were shifted laterally by 3 cm and vertically by 2 cm from the central position. The "return electrode" was located in the midline of the forehead or buccinator muscle (right/left), as shown in Figs. 3 and 6 [16,18,19,43–46].

Table 1. Tissue conductivities

Tissues	Conductivity (S/m)
Skull (bone cancellous)	0.04
Skull (bone cortical)	0.01
Blood	0.7
Cerebellum gray matter	0.1
Cerebellum white matter	0.1
Cerebrospinal fluid	1.6
Eye (vitreous)	1.6
Fat	0.08
Gray matter	0.12
Muscle	0.2
Muscle (transversal)	0.2
Muscle (longitudinal)	0.2
Skin	0.003
White matter	0.07

2.3 Registration Method

The cerebellar surface of each subject was automatically registered by an affine transformation to the standard cerebellar template (cerebellar surface representation of the MNI ICBM 2009a standard template, 0.5-mm resolution in MNI coordinates) [47,48]. Affine transformation was obtained by registering the inner surface of the skull to that of the MNI head. Iterative closest point transform of the Visualization Toolkit (VTK) was used for this registration.

For each point y in the standard cerebellar template surface Y, we found the closest point x in the registered individual cerebellum X by the means of the minimum Euclidian distance ($f: Y \rightarrow X$). If E is the EF magnitude from individual cerebellum, the template EF at y is calculated by $E\big(f(y)\big)$. The process is summarized in Fig. 2 (A). It is possible that some points on the individual surface were not assigned to the standard cerebellar template with the potential loss of hotspots or EF information due to the minimum Euclidian distance criteria. We defined a metric of the registration error to investigate the potential information loss. The registration error for each subject was the normalized mean absolute error between two EF distributions: (i) $E(x)$ which is the original EF in the individual cerebellum and (ii) $E\left(f\big(g(x)\big)\right)$ which is the registration of $E\big(f(y)\big)$ back to the individual cerebellum using the Euclidean distance ($g: X \rightarrow Y$).

$$\text{Registration Error} = 100 \times \frac{\sum_{i=}^{n} \left| E(x_i) - E\left(f\big(g(x_i)\big)\right) \right|}{n \times \max\limits_{i=1,..,n} E(x_i)} \tag{3}$$

The corresponding volumetric standard cerebellar template with 1-mm resolution was parcellated into seven functional networks (labeled C1–C7 in Fig. 2 (B)) based on the 1000 subjects by using a clustering approach [27,28], which is available in FreeSurfer (http://www.freesurfer.net/fswiki/CorticalParcellation_Yeo2011). The volumetric voxel

description of the individual cerebellum was affine transformed to the volumetric voxel description of the parcellated cerebellar template. The transformed individual cerebellum had a linear correspondence (one-to-one voxel) to the volumetric parcellated cerebellar template for group analysis in Fig. 5.

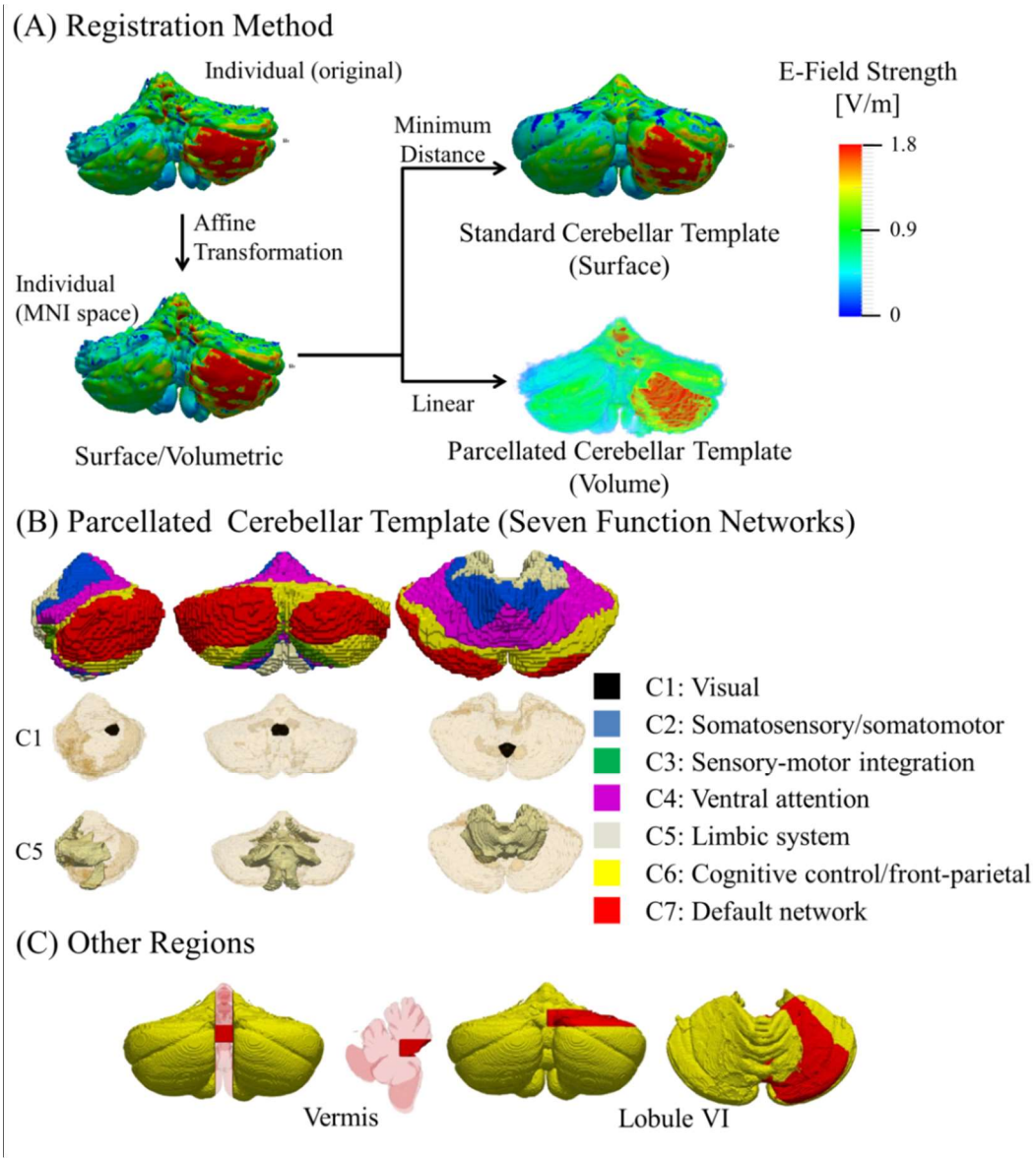

Figure 2. (A) Registration method. (B) Volumetric parcellated cerebellar template divided into seven functional networks. (C) Other regions of interest.

2.4 Analysis Methods

The spatial maximum and averaged EFs were calculated in the whole cerebellum or the subregions. The maximum EF describes the hotspot localization, whereas the average EF is a determinant of neuromodulation intensity in a specific region. To minimize inter-individual effects, the group-level EF was obtained by averaging the EF in the standard cerebellar template of all the subjects (point-to-point), as shown in Fig. 3 (B1). The inter-individual effect was quantified by the relative standard deviation of the EFs, as shown in Fig. 3 (B2). To analyze the causes of inter-individual variation, linear regression was used between the EF and individual anatomical factors. These factors include: (i) the distance between the location of the maximum EF on the cerebellum surface and the skin/skull point at the center of the electrode; (ii) the thickness of the local tissues (scalp, muscle, and skull); (iii) the circumference, length, and width of the head; and (iv) the inter-electrode distance. The local thickness was the average thickness in the cerebellar area. The cerebellar area was demarcated manually by a rectangular area that covers the cerebellum from the posterior side. Head model circumference is defined as the sum of the lengths of the temporal lines of EEG: from Fpz to T7 to Oz and from Fpz to T8 to Oz. Moreover, we considered the local and total CSF volumes, as well as the total intracranial volume, as shown in Fig. 1 (B). The local CSF volume was calculated by considering only the CSF over the cerebellum.

The EF distribution (maximum and average across all subjects) over each functional network of the cerebellum was used for statistical analysis, as shown in Fig 2 (B). Paired *t*-tests were performed to study the significance of the difference between EFs in the cerebellar regions for each montage. In total, 462 *t*-tests were performed. The Holm–Bonferroni method was used to correct the *P* values for multiple comparisons, and $p \leq 0.05$ was considered to be significant. All the analyses were performed using MATLAB (Version 2017a, Mathworks Inc., Natick, MA, USA). Additionally, averages of the EF intensities were obtained to determine the focality on

the lobule VI and vermis regions, as shown in Fig. 2 (C). The cerebellar subregions of lobule VI and vermis were selected manually from prior anatomical information [20] and confirmed by one of the co-authors who is board-certified physician on clinical physiology and cerebrovascular diseases.

3. Results

3.1. EF Distribution at Group Level

Figure 3 (A) shows that the effect of individual variability on the EF distribution of the cerebellar surface is large for an exemplary electrode montage. In some of the subjects, a non-symmetric distribution between left and right cerebellar hemispheres is found. Additionally, a considerable variability for the maximum EF is found among the subjects: 1.81 V/m ± 15% (relative standard deviation). The individual cerebellar EFs were transformed to the standard cerebellar template for group-level analysis. As shown in Figure 3(A), the registered EF distributions closely matched those on the individual cerebellar surfaces. On average, the registration error of the EFs was 6.5% (range: 4.9 – 8.0%). Registration underestimated the maximum EF on average by 0.4% (range: 0 – 1.6%). Therefore, potential information loss due to the registration was marginal.

Figure 3 (B1) shows the group-averaged (n = 18) EF distribution on the standard cerebellar template. As shown in Fig. 3, high EFs are distributed over large regions. The dominant factor affecting the field distribution (around the maximum value) is the position where the active electrode is close to the cerebellum. The peak value appears immediately under the corresponding electrode for all of the 15 montages considered here. The effect of the position of the return electrode is marginal, except when the return electrode is placed on the forehead. Figure 3 (B2) shows the relative standard deviation of the EFs, which has a maximum value of

55%.

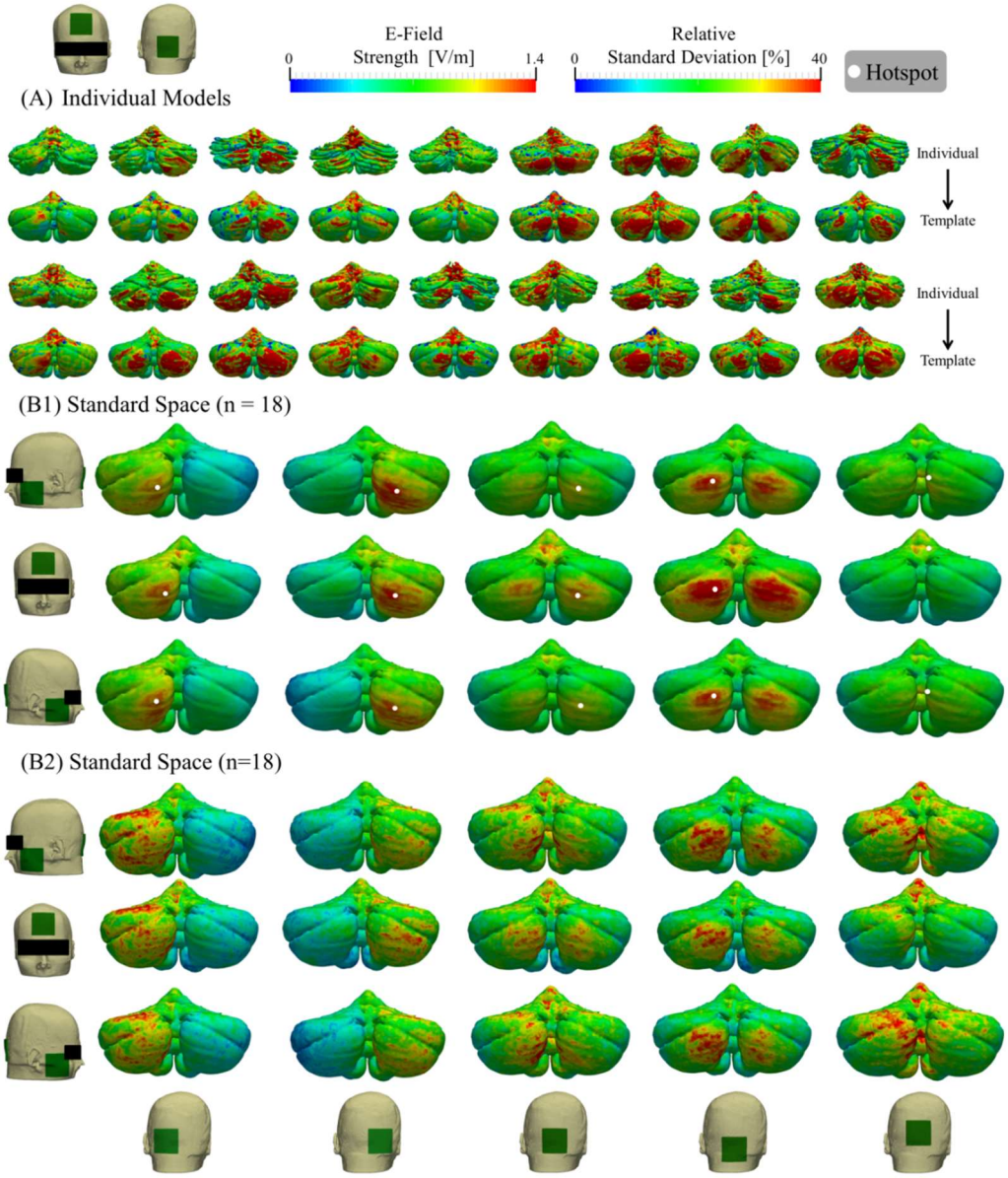

Figure 3. EF distribution. (A) Individualized EF in the cerebellum of each head model transformed on the standard cerebellar template for an exemplary electrode montage. (B1) EF averaged over different models (n = 18) in the standard cerebellar template for 15 electrode montages. (B2) Relative standard deviation of the EF (n = 18). Hotspots corresponds to the center of regions with threshold of 0.9× EF_{max}.

3.2. Variability of EF

Linear regression was used to analyze the causes of inter-individual variation of the maximum and average EF values in the cerebellum. Scatter plots of the EFs with the results of the single linear regression analysis for 18 subject-specific factors are shown in Fig. 4. Figure 4 (A) shows a statistically significant correlation between the maximum EF and the skin–cerebellum distance (R^2 = 0.62, P < 0.001), skull–cerebellum distance (R^2 = 0.43, P = 0.004), and the head circumference (R^2 = 0.45, P = 0.002). The individual EF cerebellar maps are sorted in descending order of skin–cerebellum distance (from left to right and from top to bottom) in Figure 3 (A). The local thickness of the scalp, skull, and muscle does not explain the variability of the EF. Moreover, statistically significant correlations exist between the average EF in the cerebellum and the local (R^2 = 0.67, P < 0.001) and total (R^2 = 0.53, P < 0.001) CSF volumes, as shown in Fig. 4 (B).

3.3. EF at Functional Network of Cerebellum

Figure 5 presents the modeled EFs for each montage and cerebellar region. The statistical significance of montage-wise differences is included for both the average and maximum EFs within each region. As shown in Fig. 5 (A), the effect of electrode montage on the EF is generally not significant for the maximum EF. Considerably less variation (i.e., fewer significant differences between regions) is observed in the maximum EFs within each region, where significant differences are mostly found between C1 and C2, C4, C6, and C7 for two electrode montages.

For the average EFs, as shown in Fig. 5 (B), the EF within region C5 (limbic system) was found to differ significantly from the fields in all other regions, regardless of the electrode montage. The average EFs in this region were systematically lower than those in the other regions, most likely owing to the depth of its location.

These tendencies can also be confirmed from Fig. 5 (C), where the active (occipital) electrode is shifted up/down.

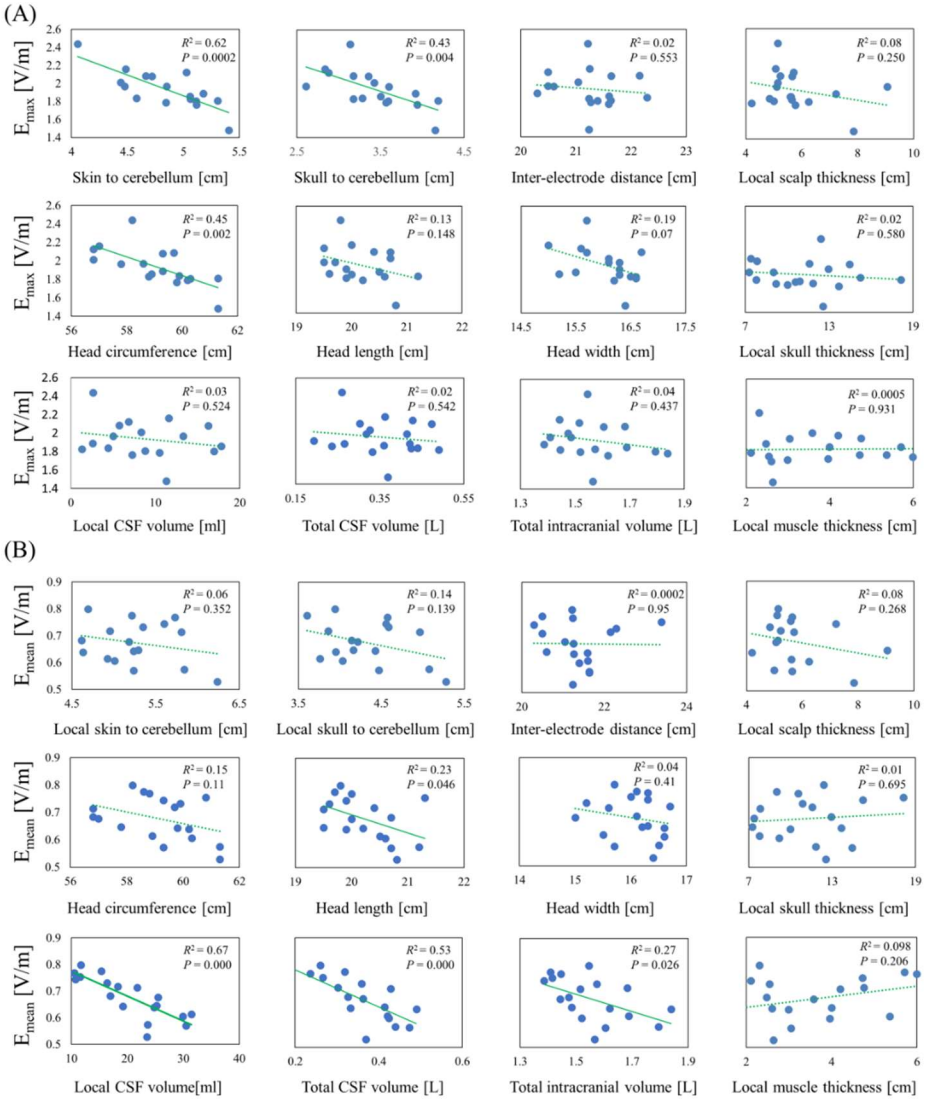

Figure 4. Relationship between the maximum (A) and average (B) EF and inter-individual anatomical factors for the active electrode at the central position and a return electrode on the forehead. Solid and dotted lines represent $P \leq 0.05$ and $P > 0.05$.

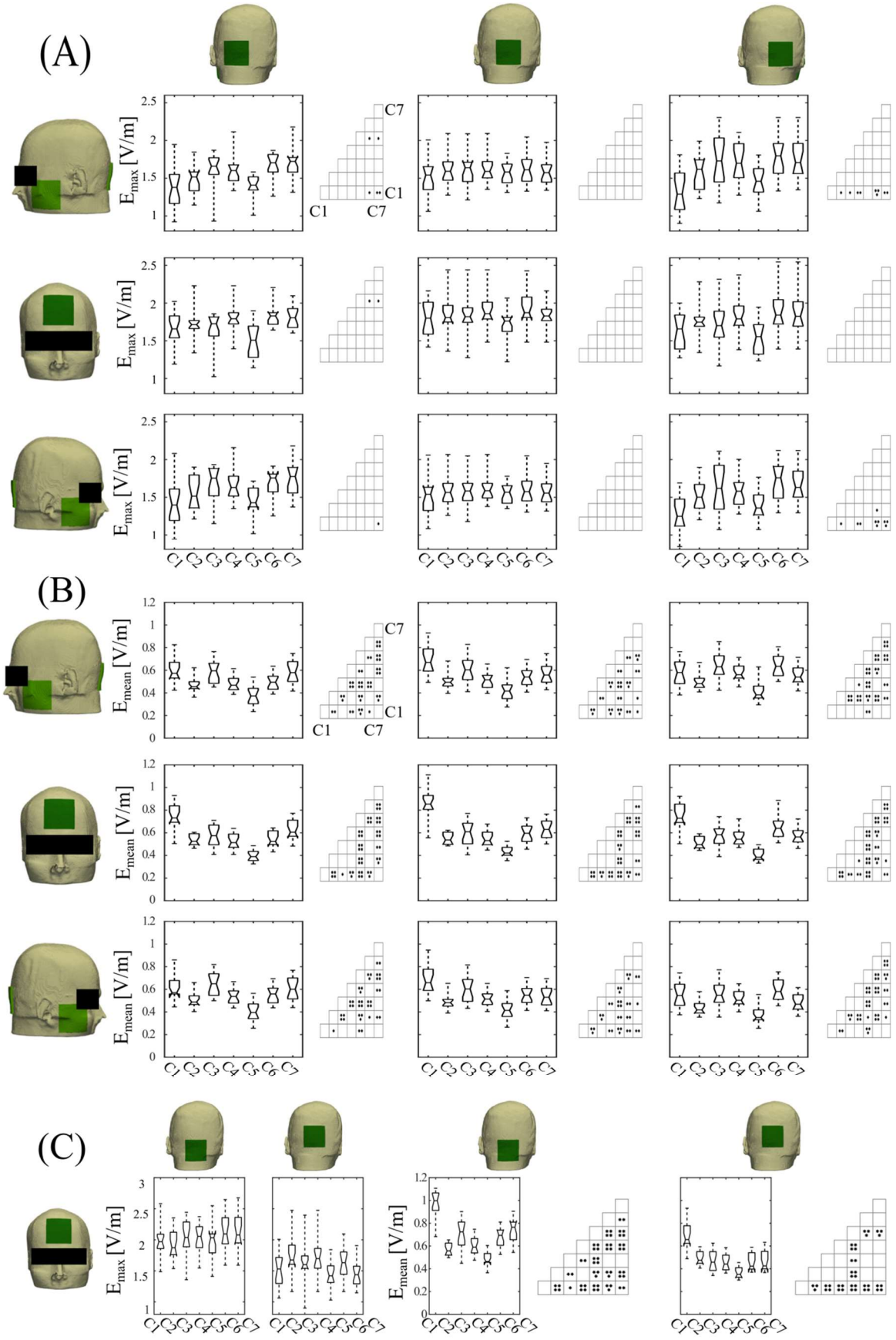
(A)
(B)
(C)
E_{max} [V/m]
E_{mean} [V/m]
C1
C7
C1 C2 C3 C4 C5 C6 C7

Figure 5. EF magnitudes in different functional networks of the cerebellum. (A) Maximum and (B) average EF for 9 different electrode montages. (C) Maximum and average EF when the active electrode at the central position is shifted up/down by 2 cm. *$P < 0.05$, **$P < 0.01$, ***$P<0.001$, ****$P < 0.0001$.

3.4. Vermis and lobule VI

Figure 6 shows that montage C-r_d (the return electrode on the forehead and the active electrode on the cerebellar right hemisphere) produced the maximum EF in lobule VI (right side), and high EFs are also produced in other regions. The montage that produced the maximum EF with the best focality was C-c_d for lobule VI. For the same region, montage C-r_2 delivered the highest average EF with the best focality. In the case of the vermis, the highest maximum and averaged EFs correspond to the C-c_d arrangement. The best focality was achieved for R-c_u or L-c_u.

3.5. Tissue anisotropy

The effect of the EF can be affected by the anisotropic characteristics of the tissues. Figure 7 shows cases of muscle anisotropy in different increasing volumes around the cerebellum. In the lateral view, the volume increases until the most posterior and anterior points and the middle point of the cerebellum. Also, the whole muscle was considered. The maximum EFs are attenuated by a maximum of 12%, whereas the mean EF is reduced by less than 7%, as presented in Table 2.

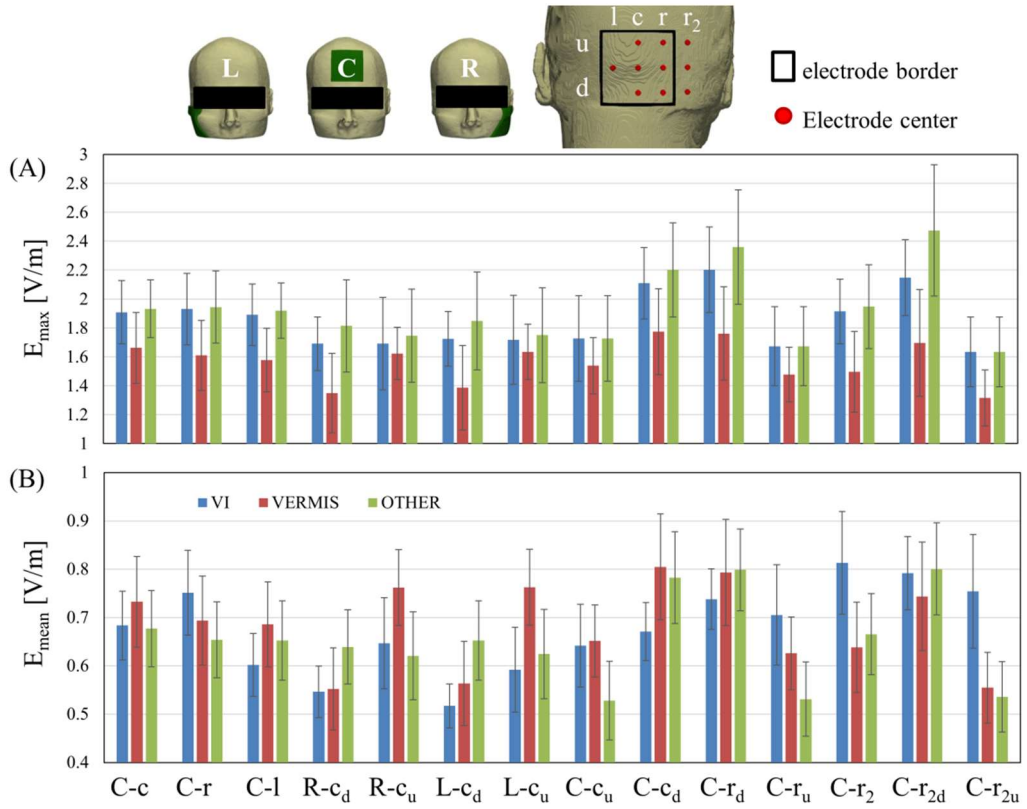

Figure 6. EF magnitudes in the vermis and lobule VI of the cerebellum. "Other" indicates regions excluding lobule VI and the vermis. (A) Maximum and (B) average EF.

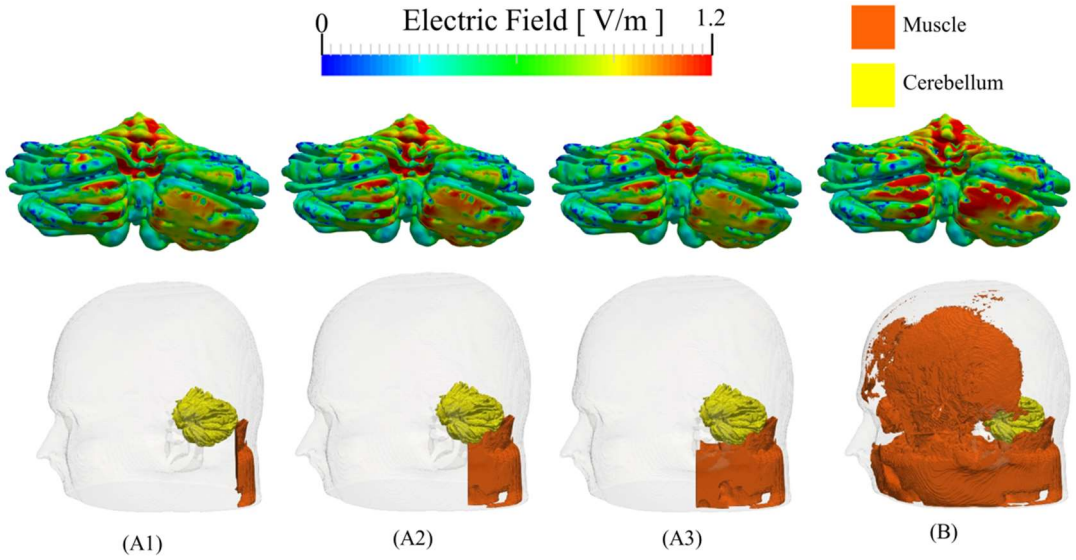

Figure 7. Effect of muscle anisotropy in three subregions (A1–A3) of the total muscle tissue. (B) Isotropic muscle tissue.

Table 2. Variation of the EF as a function of muscle anisotropy according to the models shown in Fig. 7

Model	Conductivity	E_{max} [V/m]			E_{mean} ± standard deviation [V/m]		
Anisotropic ratio		1.5	3.5	5.5	1.5	3.5	5.5
(A1)		1.75	1.66	1.66	0.60 ± 0.22	0.58 ± 0.20	0.58 ± 0.21
(A2)	Anisotropic	1.73	1.66	1.64	0.60 ± 0.21	0.58 ± 0.20	0.57 ± 0.20
(A3)		1.73	1.69	1.64	0.59 ± 0.21	0.59 ± 0.21	0.57 ± 0.20
(B)	Isotropic		1.84			0.61 ± 0.21	

4. Discussion

We computed the EF, which is a primary determinant of neuromodulation [24,40,49–52], for ctDCS in different cerebellum regions of 18 anatomical human-head models. Figure 3 (A) suggests the necessity of group-level analysis, in view of the large individual variability of the EF. This tendency is similar to that observed in motor and frontal tDCS [11,42]. For the first time, the EFs on the standard cerebellar template was used to study EF characteristics at a group level by considering different electrode montages. Moreover, we investigated the relationship between the individual anatomical variability and the EF and considered the ctDCS focality on different functional networks of the cerebellum.

We observed a systematic tendency of the stimulation hotspot for the EF distribution on the cerebellum surface at the group level, with a high EF immediately below the active electrode (Fig. 3 (B)). We also found that the relative standard deviation of the distribution of the EFs was up to 55% on the cerebellar surface. The dominant factor, which explains 62% of the variability of the maximum EFs, was the skin–cerebellum distance, as shown in Fig. 4 (A). Similarly, the skull–cerebellum distance and head circumference were also statistically significant. However,

as expected, the skull–cerebellum distance and the head circumference were related with the scalp–cerebellum distance, as shown in Fig 4. Overall, the distance of the cerebellum from the electrode influences maximum EFs.

We found that the relative standard deviation of 55% was almost three times larger than that obtained for tDCS on the motor hand area [11]. The larger variability can be explained by the skin–cerebellum distance being up to three times larger than the skin–hand motor area distance. On the other hand, the mean value of the EF in the cerebellum was significantly correlated with the average volume of the CSF, as shown in Fig. 4 (B). One possible reason for this is that the electrical conductivity of the CSF (1.6 S/m) is higher than that of the remaining brain tissue (0.07–0.12/ S/m). Hence, the electric current flows along the CSF, resulting in low cerebellar EF, which represents a reduction of the mean EF. The electrode size in this study was 6×6 cm^2. We consider the maximum and mean EFs for different electrode areas (2×2 cm^2 to 5×5 cm^2) in the Appendix B. There was a significant difference of the maximum EFs (20% of variation between smaller and the largest electrode), but marginal difference of the maximum EFs between 5×5 cm^2 and 6×6 cm^2 (relative difference lower than 3%). Also, the variations of the mean EFs and hotspot locations were marginal.

Although current spread to other brain structures outside the cerebellum is unlikely to produce functional effects [53], how the current spreads in functional networks inside the cerebellum has not been investigated. The EF distributions were obtained in seven functional networks of a parcellated cerebellum. Figure 5 (A) suggests that focal stimulation on different functional networks of the cerebellum is difficult, at least in terms of the maximum EF, based on group-level analysis. In contrast, functional network analysis becomes important when the mean EF is used as a metric of the ctDCS dosage. Similarly, dosage control for specific regions (e.g., the vermis and lobule VI) can be achieved by customized montages, which can be useful for

improving motor deficiencies in limb control and walking in patients with neurological disorders. It should be noted, however, that the selection of the electrode montage requires a trade-off between the maximum stimulation dosage area and focality, as shown in Fig. 6.

Although the EF strength is not the only factor affecting neural activation, the final effects of tDCS would also depend on the physiological (e.g., genetics, sex, and age) and cognitive state of the subject [54,55]. A large range of uncertainty exists in the in vivo electrical conductivity of tissues in particular at extremely low frequencies and skin tissue [56]. However, different sets of conductivities did not modify the EF distributions (Appendix C). Moreover, we considered the anisotropy of the muscle tissue. A maximum variation of 12% was obtained for the EFs between anisotropic and isotropic muscle tissues, so no consideration of the anisotropic muscle tissue may have a limited impact of the variability presented here (Fig. 7). Another factor that we did not consider here is the effect of anisotropy in the cerebellar and brain tissue [25], in which further variability can be expected in particular for EF distributions in particular for subcortical regions [57].

5. Conclusions

The different distributions of the EFs during cerebellar tDCS are due to inter-individual differences. Variations of the EF on the cerebellar surface were found to have standard deviations of up to 55% of the mean. The dominant anatomical factor explaining this variability was the skin–cerebellum distance for the maximum EF and the local CSF volume for distributions inside the cerebellum. Despite the inter-individual variations, we were able to determine a systematic tendency of the EF hotspot to emerge beneath the active electrode in group-level analysis. Finally, electrode localization can be adjusted to target specific positions, so that the most effective stimulation is delivered to a group of subjects.

Declarations of interest: none

Acknowledgments

JSPS Grant-in-Aid for Scientific Research (A), JSPS KAKENHI 17H00869.

Appendix A: Head Models with average neck

Due to the limited field of view in the neck, an average neck of seven subjects was added to the models for ctDCS. In brief, the average neck image was generated in the following way [11]: First, the MR images of seven subjects with neck were registered to the MNI template using affine registration, and the average was taken resulting in an average image in MNI space, which also included an average image of the neck. When adding the average neck, the subject images without neck were first affinely registered to the MNI space. Then the inverse transformation was used to map the average neck to the subject images. The boundary between the subject images and the average neck was smoothed to prevent the formation of sharp edges.

To investigate the effect of adding the average neck, we used five subjects whose images included the neck. The subject images were modified to replace the original neck with the average neck. We then compared the EFs calculated in models with the average neck (AvN) with those calculated in the models with the original neck (OrN). The relative difference of the maximum EF between OrNs and AvNs was less than 2% . Likewise, the relative difference of the mean EF was lower than 4%. Also, the group-level EF of OrNs and AvNs did not show a significant difference in the standard cerebellar template around the hotspots.

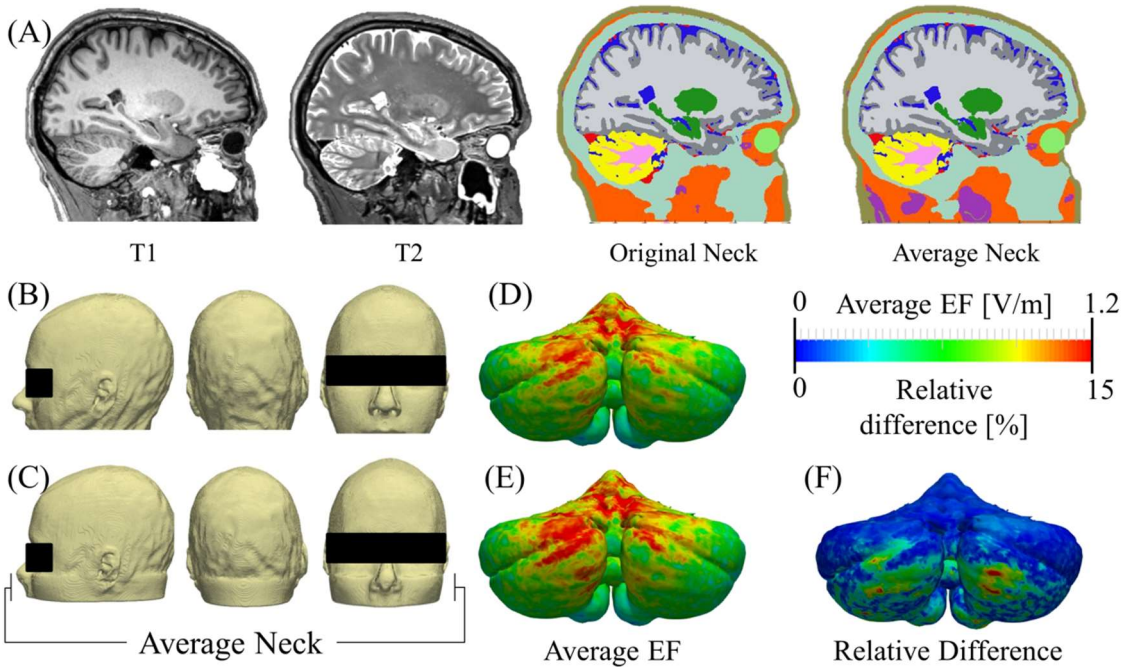

Figure A1. Effect of the average neck. (A) MRI data and segmentation of head model with original neck and average neck. (B) 3D head model with original neck. (C) 3D head model with the average neck. (D) Group-level EF of the head models with original neck. (E) Group-level EF of the head models with the average neck. (F) The relative difference between D and E. Montage corresponds to active electrode over the center of the cerebellum and return electrode on the forehead.

Appendix B: Electrode size effect

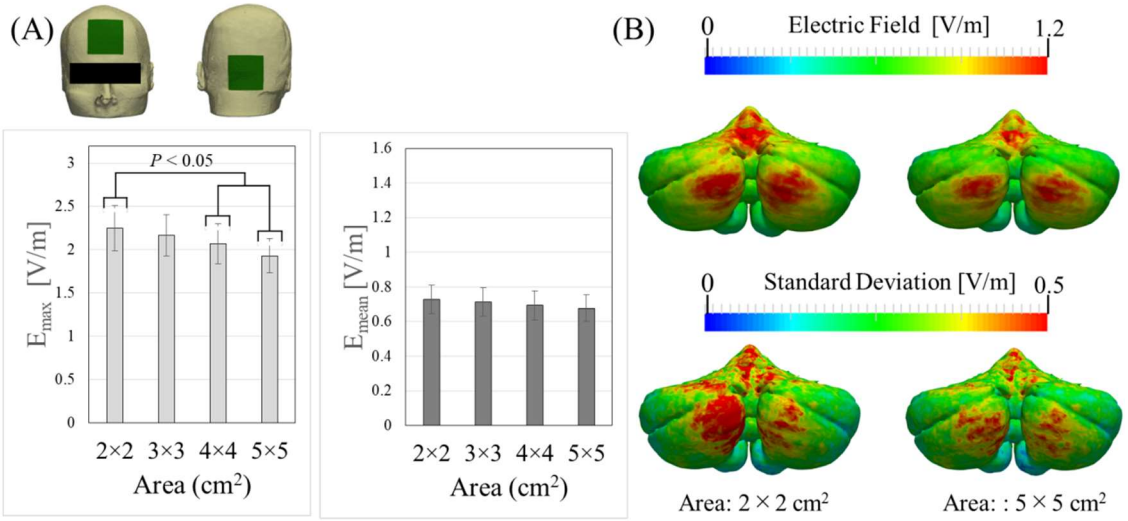

Figure B1. (A) Distribution of maximum and mean EFs (n = 18) using different electrode sizes (2–5 cm in length). The average EF and the corresponding standard derivation on the cortical surface are also shown. A one-way ANOVA test ($F(3,68) = 5.34$, $P < 0.01$), followed by Bonferroni-corrected post hoc t-tests, showed significant differences between the 4-cm^2 electrodes and the 16–25-cm^2 electrodes for the maximum EF. The difference among electrode areas for the mean EF was not statistically significant ($F(3,68) = 1.31$, $P = 0.28$). (B) EFs (n = 18) in cerebellar cortex indicates similar hotspots position. However, a larger variability is observed using smaller electrode size.

Appendix C: Effect of conductivity variation

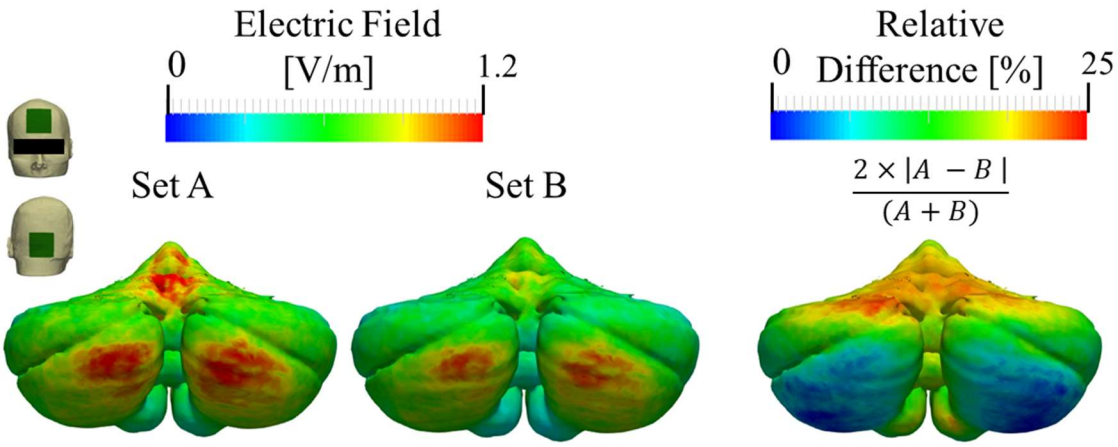

Figure C1. Group analysis of averaged EF distributions (n = 18) for two different conductivity sets (A: current study and B: Ref. [42]). The difference between the two sets is 0.10 ± 0.07 V/m in the cerebellar surface and their relative difference is up to 25%. There is relative difference between the two sets of conductivities values of 50% for grey and white matter, 40% for cancellous bone, and 20% for dura, cortical bone and fat tissues. We believe that this conductivities values change is significant to investigate the effect of conductivity variation.

References

[1] Ugawa Y, Day B L, Rothwell J C, Thompson P D, Merton P A and Marsden C D 1991 Modulation of motor cortical excitability by electrical stimulation over the cerebellum in man. *J. Physiol.* **441** 57–72

[2] Ugawa Y, Uesaka Y, Terao Y, Hanajima R and Kanazawa I 1995 Magnetic stimulation over the cerebellum in humans *Ann. Neurol.* **37** 703–13

[3] Opitz A, Paulus W, Will S, Antunes A and Thielscher A 2015 Determinants of the electric field during transcranial direct current stimulation *Neuroimage* **109** 140–50

[4] Miranda P C, Mekonnen A, Salvador R and Ruffini G 2013 The electric field in the cortex during transcranial current stimulation *Neuroimage* **70** 48–58

[5] Datta A, Bansal V, Diaz J, Patel J, Reato D and Bikson M 2009 Gyri-precise head model of transcranial direct current stimulation: Improved spatial focality using a ring electrode versus conventional rectangular pad *Brain Stimul.* **2**201–207.e1

[6] Nitsche M A, Cohen L G, Wassermann E M, Priori A, Lang N, Antal A, Paulus W, Hummel F, Boggio P S, Fregni F and Pascual-Leone A 2008 Transcranial direct current stimulation: State of the art 2008 *Brain Stimul.* **1** 206–23

[7] Gomez-Tames J, Sugiyama Y, Laakso I, Tanaka S, Koyama S, Sadato N and Hirata A 2016 Effect of microscopic modeling of skin in electrical and thermal analysis of transcranial direct current stimulation *Phys. Med. Biol.* **61** 8825–38

[8] Ramaraju S, Roula M A and McCarthy P W 2018 Modelling the effect of electrode displacement on transcranial direct current stimulation (tDCS) *J. Neural Eng.* **15** 16019

[9] Guler S, Dannhauer M, Erem B, Macleod R, Tucker D, Turovets S, Luu P, Erdogmus D and Brooks D H 2016 Optimization of focality and direction in dense electrode array transcranial direct current stimulation (tDCS) *J. Neural Eng.* **13** 36020

[10] Huang Y, Dmochowski J P, Su Y, Datta A, Rorden C and Parra L C 2013 Automated MRI segmentation for individualized modeling of current flow in the human head *J. Neural Eng.* **10** 66004

[11] Laakso I, Tanaka S, Koyama S, De Santis V and Hirata A 2015 Inter-subject variability in electric fields of motor cortical tDCS *Brain Stimul.* **8** 906–13

[12] Kessler S K, Minhas P, Woods A J, Rosen A, Gorman C and Bikson M 2013 Dosage Considerations for Transcranial Direct Current Stimulation in Children: A Computational Modeling Study ed C Chambers *PLoS One* **8** e76112

[13] Coffman B A, Clark V P and Parasuraman R 2014 Battery powered thought: Enhancement of attention, learning, and memory in healthy adults using transcranial direct current stimulation *Neuroimage* **85** 895–908

[14] Mikkonen M, Laakso I, Sumiya M, Koyama S, Hirata A and Tanaka S 2018 TMS motor thresholds correlate with TDCS electric field strengths in hand motor area *Front. Neurosci.* **12** 426

[15] Ferrucci R, Bocci T, Cortese F, Ruggiero F and Priori A 2016 Cerebellar transcranial direct current stimulation in neurological disease. *Cerebellum & ataxias* **3** 16

[16] Grimaldi G, Argyropoulos G P, Bastian A, Cortes M, Davis N J, Edwards D J, Ferrucci R, Fregni F, Galea J M, Hamada M, Manto M, Miall R C, Morales-Quezada L, Pope P A, Priori A, Rothwell J, Tomlinson S P and Celnik P 2016 Cerebellar Transcranial Direct Current Stimulation (ctDCS) *Neurosci.* **22** 83–97

[17] Boehringer A, Macher K, Dukart J, Villringer A and Pleger B 2013 Cerebellar Transcranial Direct Current Stimulation Modulates Verbal Working Memory *Brain Stimul.* **6** 649–53

[18] Jayaram G, Tang B, Pallegadda R, Vasudevan E V L, Celnik P and Bastian A 2012

Modulating locomotor adaptation with cerebellar stimulation *J. Neurophysiol.* **107** 2950–7

[19] Galea J M, Vazquez A, Pasricha N, de Xivry J-J O and Celnik P 2011 Dissociating the roles of the cerebellum and motor cortex during adaptive learning: the motor cortex retains what the cerebellum learns. *Cereb. Cortex* **21** 1761–70

[20] Coffman K A, Dum R P and Strick P L 2011 Cerebellar vermis is a target of projections from the motor areas in the cerebral cortex *Proc. Natl. Acad. Sci.* **108** 16068–73

[21] Chambers W W and Sprague J M 1955 Functional localization in the cerebellum. I. Organization in longitudinal cortico-nuclear zones and their contribution to the control of posture, both extrapyramidal and pyramidal *J. Comp. Neurol.* **103** 105–29

[22] Chambers W W and Sprague J M 1955 Functional localization in the cerebellum. II. Somatotopic organization in cortex and nuclei. *AMA. Arch. Neurol. Psychiatry* **74** 653–80

[23] Parazzini M, Fiocchi S, Liorni I, Priori A and Ravazzani P 2014 Computational modeling of transcranial direct current stimulation in the child brain: implications for the treatment of refractory childhood focal epilepsy *Int. J. Neural Syst.* **24** 1430006

[24] Fiocchi S, Ravazzani P, Priori A and Parazzini M 2016 Cerebellar and Spinal Direct Current Stimulation in Children: Computational Modeling of the Induced Electric Field. *Front. Hum. Neurosci.* **10** 522

[25] Rampersad S M, Janssen A M, Lucka F, Aydin U, Lanfer B, Lew S, Wolters C H, Stegeman D F and Oostendorp T F 2014 Simulating Transcranial Direct Current Stimulation With a Detailed Anisotropic Human Head Model *IEEE Trans. Neural Syst. Rehabil. Eng.* **22** 441–52

[26] Fiocchi S, Longhi M, Ravazzani P, Roth Y, Zangen A and Parazzini M 2016 Modelling of the Electric Field Distribution in Deep Transcranial Magnetic Stimulation in the Adolescence, in the Adulthood, and in the Old Age *Comput. Math. Methods Med.* **2016** 1–9

[27] Buckner R L, Krienen F M, Castellanos A, Diaz J C and Yeo B T T 2011 The organization of the human cerebellum estimated by intrinsic functional connectivity *J. Neurophysiol.* **106** 2322–45

[28] Thomas Yeo B T, Krienen F M, Sepulcre J, Sabuncu M R, Lashkari D, Hollinshead M, Roffman J L, Smoller J W, Zöllei L, Polimeni J R, Fischl B, Liu H and Buckner R L 2011 The organization of the human cerebral cortex estimated by intrinsic functional connectivity *J. Neurophysiol.* **106** 1125–65

[29] Dale A M, Fischl B and Sereno M I 1999 Cortical Surface-Based Analysis *Neuroimage* **9** 179–94

[30] Fischl B 2012 FreeSurfer *Neuroimage* **62** 774–81

[31] Dawson T W and Stuchly M A 1998 High-resolution organ dosimetry for human exposure to low-frequency magnetic fields *IEEE Trans. Magn.* **34** 708–18

[32] Gabriel S, Lau R W and Gabriel C 1996 The dielectric properties of biological tissues: III. Parametric models for the dielectric spectrum of tissues *Phys. Med. Biol.* **41** 2271

[33] Yamamoto T and Yamamoto Y 1976 Electrical properties of the epidermal stratum corneum *Med. Biol. Eng.* **14** 151–8

[34] Hart F X, Berner N J and McMillen R L 1999 Modelling the anisotropic electrical properties of skeletal muscle *Phys. Med. Biol.* **44** 413–21

[35] Tarulli A W, Chin A B, Partida R A and Rutkove S B 2006 Electrical impedance in bovine skeletal muscle as a model for the study of neuromuscular disease *Physiol. Meas.*

27 1269–79

[36] Chin A B, Garmirian L P, Nie R and Rutkove S B 2008 Optimizing measurement of the electrical anisotropy of muscle *Muscle Nerve* **37** 560–5

[37] Aaron R, Huang M and Shiffman C A 1997 Anisotropy of human muscle via non-invasive impedance measurements. *Phys. Med. Biol.* **42** 1245–62

[38] Laakso I and Hirata A 2012 Fast multigrid-based computation of the induced electric field for transcranial magnetic stimulation *Phys. Med. Biol.* **57** 7753–65

[39] Gomez-Tames J, Laakso I, Haba Y, Hirata A, Poljak D and Yamazaki K 2017 Computational Artifacts of the In Situ Electric Field in Anatomical Models Exposed to Low-Frequency Magnetic Field *IEEE Trans. Electromagn. Compat.* **60** 589–97

[40] Saturnino G B, Antunes A and Thielscher A 2015 On the importance of electrode parameters for shaping electric field patterns generated by tDCS *Neuroimage* **120** 25–35

[41] Dundas J E, Thickbroom G W and Mastaglia F L 2007 Perception of comfort during transcranial DC stimulation: Effect of NaCl solution concentration applied to sponge electrodes *Clin. Neurophysiol.* **118** 1166–70

[42] Laakso I, Tanaka S, Mikkonen M, Koyama S, Sadato N and Hirata A 2016 Electric fields of motor and frontal tDCS in a standard brain space: A computer simulation study *Neuroimage* **137** 140–51

[43] Dutta A, Paulus W and Nitsche M A 2014 Facilitating myoelectric-control with transcranial direct current stimulation: a preliminary study in healthy humans *J. Neuroeng. Rehabil.* **11** 13

[44] Grimaldi G and Manto M 2013 Anodal Transcranial Direct Current Stimulation (tDCS) Decreases the Amplitudes of Long-Latency Stretch Reflexes in Cerebellar Ataxia *Ann. Biomed. Eng.* **41** 2437–47

[45] Ferrucci R, Cortese F and Priori A 2015 Cerebellar tDCS: How to Do It *The Cerebellum* **14** 27–30

[46] Cantarero G, Spampinato D, Reis J, Ajagbe L, Thompson T, Kulkarni K and Celnik P 2015 Cerebellar direct current stimulation enhances on-line motor skill acquisition through an effect on accuracy. *J. Neurosci.* **35** 3285–90

[47] Fonov V, Evans A, McKinstry R and Almli C 2009 Unbiased nonlinear average age-appropriate brain templates from birth to adulthood *Neuroimage* **47** S102

[48] Fonov V, Evans A C, Botteron K, Almli C R, McKinstry R C, Collins D L and Brain Development Cooperative Group 2011 Unbiased average age-appropriate atlases for pediatric studies *Neuroimage* **54** 313–27

[49] Miranda P C, Callejón-Leblic M A, Salvador R and Ruffini G 2018 Realistic modeling of transcranial current stimulation: The electric field in the brain *Curr. Opin. Biomed. Eng.* **8** 20–7

[50] Priori A, Ciocca M, Parazzini M, Vergari M and Ferrucci R 2014 Transcranial cerebellar direct current stimulation and transcutaneous spinal cord direct current stimulation as innovative tools for neuroscientists. *J. Physiol.* **592** 3345–69

[51] Bikson M and Datta A 2012 Guidelines for precise and accurate computational models of tDCS *Brain Stimul.* **5** 430–1

[52] Woods A J, Antal A, Bikson M, Boggio P S, Brunoni A R, Celnik P, Cohen L G, Fregni F, Herrmann C S, Kappenman E S, Knotkova H, Liebetanz D, Miniussi C, Miranda P C, Paulus W, Priori A, Reato D, Stagg C, Wenderoth N and Nitsche M A 2016 A technical guide to tDCS, and related non-invasive brain stimulation tools *Clin. Neurophysiol.* **127** 1031–48

[53] Parazzini M, Rossi E, Ferrucci R, Liorni I, Priori A and Ravazzani P 2014 Modelling

the electric field and the current density generated by cerebellar transcranial DC stimulation in humans *Clin. Neurophysiol.* **125** 577–84

[54] Li L M, Uehara K and Hanakawa T 2015 The contribution of interindividual factors to variability of response in transcranial direct current stimulation studies *Front. Cell. Neurosci.* **9** 181

[55] Chew T, Ho K-A and Loo C K 2015 Inter- and Intra-individual Variability in Response to Transcranial Direct Current Stimulation (tDCS) at Varying Current Intensities *Brain Stimul.* **8** 1130–7

[56] Huang Y, Liu A A, Lafon B, Friedman D, Dayan M, Wang X, Bikson M, Doyle W K, Devinsky O and Parra L C 2017 Measurements and models of electric fields in the in vivo human brain during transcranial electric stimulation *Elife* **6** e18834

[57] Suh H S, Lee W H and Kim T-S 2012 Influence of anisotropic conductivity in the skull and white matter on transcranial direct current stimulation via an anatomically realistic finite element head model *Phys. Med. Biol.* **57** 6961–80